Song, J.; Wang, Z.; Huang, Y.; Srinivasan, A.; Beckmann, F.; Kainer, K.U.; Hort, N.:

Effect of Zn addition on hot tearing behaviour of Mg–0.5Ca–xZn alloys

In: Materials and Design (2015) Elsevier

DOI: 10.1016/j.matdes.2015.08.026

Effect of Zn addition on hot tearing behaviour of Mg-0.5Ca-xZn alloys

Jiangfeng Song[1,*], Zhi Wang[2], Yuanding Huang[1], Amirthalingam Srinivasan[3], Felix Beckmann[1], Karl Ulrich Kainer[1], Norbert Hort[1]

1 Institute of Materials Research, Helmholtz-Zentrum Geesthacht, Max-Planck-Str. 1, 21502 Geesthacht, Germany

2 School of Materials Science and Engineering, Shenyang University of Technology, Shenyang 110870, China

3 CSIR-National Institute for Interdisciplinary Science and Technology (NIIST), Trivandrum 695019, India

Abstract

The influence of Zn addition (0, 0.5, 1.5, 4.0 and 6.0 wt. %) on hot tearing behaviour of Mg-0.5 wt.% Ca alloy was investigated using a constrained rod casting (CRC) apparatus. The effects of mould temperature and grain refinement on the hot tearing susceptibility (HTS) were studied. Hot tears were observed with 3D X-ray tomography and the tear volumes were quantified. Results show that the Zn addition increases the HTS of Mg-0.5Ca alloys. At a mould temperature of 250 ^{0}C, all alloys investigated except Mg-0.5Ca-6Zn alloy show severe HTS. An increase in the mould temperature from 250 ^{0}C to 450 ^{0}C did not reduce the HTS in Mg-0.5Ca-1.5Zn and Mg-0.5Ca-4Zn alloys. Among all the investigated alloys, Mg-0.5Ca-4Zn alloy exhibits severe HTS as it completely broke away from the sprue-rod junction. The HTS of alloys was well correlated with the susceptible temperature range (ΔT_s). An increase in ΔT_s increased the HTS. The hot tears propagated along the grain boundaries through liquid film rupture. Grain refinement by Zr addition improved the hot tearing resistance of Mg-0.5Ca-4Zn alloy as the fine grain structure facilitated the easy feeding of liquid into the last area of solidification and accommodated the developed strain more effectively.

Keywords: Hot tearing, Mg-0.5Ca-xZn alloys, 3D X-ray tomography, grain refinement, mould temperature

* Corresponding author:
Email: jiangfeng.song@hzg.de
Tel.:+49 (0) 4152 87 1912
Fax: +49 (0) 4152 87 1909

1 Introduction

Hot tearing is a major casting defect and has a significant impact on the quality of cast products [1]. It is a complex solidification phenomenon which is still not fully understood [2]. Hot tearing occurs above the solidus temperature due to obstructed contraction of the solidifying alloy, often at hot spots where the casting solidifies last or at areas where there is a sharp change of cross section [3]. Previous studies show that hot tears initiate when the liquid flowing through the mushy zone becomes insufficient to fill the cavities.

Hot tearing of several binary Mg alloys has been extensively studied, such as Mg-Al [2, 4, 5], Mg-Zn [6], Mg-Y [7], and Mg-Gd [8]. In addition, hot tearing behaviour of a few ternary alloys, Mg-Zn-Y [9, 10], Mg-Ca-Al [11], Mg-Sr-Al [3, 12], and Mg-Zn-Al [13, 14], have also been studied. Results indicated that the hot tearing susceptibility (HTS) of Mg alloys was both composition and initial mould temperature dependent. The maximum HTS of Mg- (0.5-12) wt.% Zn alloys appeared at the Zn content of 1.5 wt. % [6]. The addition of Y decreased the HTS of Mg-Zn-Y alloys, which was attributed to the shortened freezing range [9, 10]. Wang et al. [14] found that addition of Zn (0-1 wt.%) deteriorated hot tearing resistance of Mg-9Al-Zn alloys due to inter-crystalline segregation of Zn and Al. It has been reported that a high initial mould temperature significantly improved the hot tearing resistance of Mg alloys [4, 15, 16]. Wang et al. [17] also studied the effects of grain refiner (Zr) on hot tearing behaviour of Mg-Zn-Y alloys and reported that the grain refinement significantly decreased the HTS.

Mg-Zn-Ca ternary alloys have a potential to be developed for biodegradable and automotive applications. Zhang et al. [18-20] conducted a series of investigations on biodegradable ternary Mg-Zn-Ca alloys, and their results revealed that the mechanical properties can be tailored by varying Zn and Ca contents. Both *in vitro* and *in vivo* studies showed that the designated Mg-Zn-

Ca ternary alloys were biocompatible [19]. Studies also showed that Mg-Zn-Ca alloys had an excellent creep resistance [21, 22], and their mechanical properties as well as corrosion resistance can be further improved by forming [23-26], heat treatment [21, 27], and surface treatment [28]. With addition of 0.6 wt.% Zr, the tensile strength and ductility of Mg-1Ca-1Zn-0.6Zr alloy was found to superior to that of AZ91 alloy [21] and the creep resistance of Mg-1Ca-1Zn-0.6Zr alloy was also significantly better than that of AZ91 alloy at temperatures up to 150 ^{0}C [21].

As most of the magnesium alloys are prepared by casting, the high quality casting with fewer defects is desirable for the further processing or final applications. Thus, the castability of as-cast alloys, especially the resistance to hot tearing must be considered [12]. Our previous investigation on the hot tearing characteristics of Mg-xCa alloys showed that Mg-0.5 wt. % Ca exhibited the highest HTS. Considering the potential application of the Mg-Ca-Zn ternary alloys, it is of importance to investigate their hot tearing behaviour. Consequently, the effect of Zn addition on hot tearing behaviour of Mg-0.5Ca-xZn alloys was investigated in the present study.

2 Material and methods

2.1 Hot tearing casting

Pure Mg, Ca, and Zn, and Mg-33 wt.% Zr master alloy were used to prepare the ternary Mg-0.5Ca-xZn (x=0.5, 1.5, 4, and 6 wt.%) alloys and Mg-0.5Ca-4Zn-0.5Zr alloy. Approximately 350 g of Mg was melted in a mild steel crucible under a protective gas mixture of high pure Ar + 0.2% SF_6. Alloying elements were added at 700 °C and manually stirred for 2 min. Then the melt was heated to 750 °C, held at this temperature for 5 min, and cast into a constraint rod casting (CRC) mould. The mould was coated with a thin layer of boron nitride (hexagonal), and

preheated to 250 °C or 450 °C. The casting was extracted from the mould after it solidified completely. The hot tearing test was repeated at least 3 times for each alloy.

The actual chemical compositions of the castings were analysed using spark optical emission spectroscopy (OES) (Spectroflame, Spectro, Kleve, Germany), and are listed in Table 1. Most of the actual compositions were close to the nominal compositions. However, the actual Zr content was lower (0.24 wt.%) in comparison with initial addition of 0.5 wt.%.

Schematic diagram of the CRC mould as well as a complete casting is shown in Fig. 1. More detailed description about the hot tearing setup can be found in Ref. [7]. Using this setup, force and temperatures were simultaneously recorded during casting. The resulting force and temperature curves as a function of time were later used to analyse the initiation of hot tearing. Three thermocouples (TC 1, TC 2, and TC 3) were used to measure the temperature during solidification and their locations in the mould are shown in Fig. 1 (a). All thermocouples were protected with steel tubes. A steel screw located at the rear end of the rod portion of the mould and was used to connect the casting to the load sensor. Part of the steel screw was inserted into the mould, such a way that the liquid metal solidified over it and hence the load cell could measure the stress developed during solidification (Fig. 1 (b)).

2.2 Hot tear evaluation

The castings were initially visually inspected for hot tears and photographed with a digital camera. They were then observed more in detail with 3D X-ray micro-tomography technique. With this technique, 3D images of the tears can be obtained, which provides three dimensional distributions of tears in the casting. Additionally, the complete tear volume, including both the closed and open tears, can be accurately quantified.

The hot tears were evaluated in a 3D X-ray tube-based high resolution tomography (nanotom® s – phoenix, GE Measurement & Control Solutions, Germany). Detailed experimental procedure as well as data processing methods can be found elsewhere [7]. Fig. 2 shows the sample for 3D X-ray tomography measurement which was machined out of the complete casting. The sample consisted of both rod and a machined portion of the sprue of the casting (cubic shaped) and prepared such a way that the tear was in the middle portion of the sample (Fig. 2). The diameter of the rod was around 12 mm whereas the cubic portion was machined to a smallest possible size without affecting the morphology of the tear to obtain the best tomography resolution. The tear volume was calculated based on the 3D volume reconstruction results.

2.3 Characterization of microstructures and fracture surfaces

The microstructures and tear morphologies were investigated with optical microscope (OM, LEICA DMI5000 M microscope, Germany) and scanning electron microscope (SEM, Zeiss Ultra 55 SEM, Germany). The SEM is equipped with Energy Dispersive X-ray Spectroscopy (EDS). The samples for microstructural observations were cold mounted, ground with SiC abrasive paper until grit size of 2500, and polished with water free OPS and 1 μm diamond suspension. The polished samples were chemically etched in a solution of 8 g picric acid, 5 ml acetic acid, 10 ml distilled water, and 100 ml ethanol. Grain sizes were determined using the line intercept method. The fracture surfaces of castings with a severe tear were also observed by SEM.

3 Results

3.1 Optical microstructures

The grain size plays an important role on the HTS of alloys [29, 30]. Thus, grain morphologies of Mg-0.5Ca-xZn alloys cast at T_{mould} = 250 ^{0}C and T_{mould} = 450 ^{0}C were observed (Fig. 3). All

the OM pictures were taken from the rod portion near the sprue-rod junction (cut vertically along the mid plane).

The addition of Zn refined the grain sizes of Mg-0.5Ca-xZn alloys at both mould temperatures, as shown in Table 2. The grain refinement mechanism was attributed to the grain growth restriction resulting from constitutional undercooling due to the segregation of Zn during solidification. It was reported that Zn addition increased the grain growth restriction factor of Mg-0.5Ca alloys which resulted in the grain refinement [34]. However, increase in Zn content from 4 to 6 wt. % resulted in slight increase in grain size. The increase in the mould temperature increased the grain size marginally for all the alloys.

The morphology of grain in all alloys was mainly equiaxed. Dendrites could be observed inside the grains of the alloys with low Zn contents (less than 4 wt.%) cast at T_{mould} = 250 ^{0}C. It was found that dendrites were more likely to form at the lower mould temperature, which was attributed to the non-uniform distribution of the solute inside the grain due to the fast cooling.

3.2 Force-temperature-time curves

The as-recorded force-temperature-time curves of Mg-0.5Ca-xZn alloys cast at the mould temperature of 250 ^{0}C are displayed in Fig. 4. As Mg-0.5Ca alloy (Fig. 4 (a)) has a high solidus temperature of 517 ^{0}C, the force-temperature-time curve was recorded only for 695 s. The information on the initiation and propagation of hot tearing can be obtained from these curves [7], as marked on Fig. 4. Normally, a drop in the measured force on the force curve is regarded as the initiation of hot tearing, i.e. Fig. 4 (e). The force drop reveals the stress relaxation resulting from the hot tear formation [31]. Therefore, the hot tearing initiation was determined to be at the time when a drop in force was observed. However, for some alloys, for instance Mg-0.5Ca-1.5Zn and Mg-0.5Ca-4Zn alloys, no typical force drops could be found. For these two alloys (Fig. 4 (c) and

(d)), the force drop occurred at the beginning of the solidification which was due to the interaction between the liquid metal and the steel screw connected to the load cell. In these cases, the initiation of hot tearing can be identified at the point where the slop of the force curve changes significantly and suddenly. The detailed determination of hot tearing initiation in Mg0.5Ca-4Zn alloy is shown in Fig. 4 (f). Similar determination method of hot tearing initiation for some alloys investigated with CRC mould can also be found in Ref. [32].

By locating the force drop position, the corresponding temperature (T_i) at which the hot tearing initiates can be determined. Using this temperature the corresponding solid fraction (f_{si}) was calculated with Scheil's solidification model. The hot tearing initiation temperatures (T_i) and the corresponding solid fractions (f_{si}) are shown in Fig. 4. Among these, the force curve of Mg-0.5Ca and Mg-0.5Ca-0.5Zn alloys (Fig. 4 (a) and (b)) did not show any further increment in force after the tear propagation completed suggesting that the tear was so severe and the casting was completely broken. Additionally, multiple force drops was seen on the curve for Mg-0.5Ca-6Zn alloy (Fig. 4 (e)), indicating that more than one tear might have initiated during the solidification.

Fig. 5 shows the force-temperature-time curves of Mg-0.5Ca-xZn alloys cast at a mould temperature of 450 ^{0}C. Similar to the curve shown in Fig. 4 (a), the curve of Mg-0.5Ca (Fig. 5 (a)) was recorded until 1403 s. Force drops were easily observed in all the force curves. The T_i and f_{si} values of alloys are also indicated in Fig. 5. It should be noted that T_i and f_{si} values for Mg-0.5Ca-4Zn alloy were only estimated as the tear in this alloy occurred at the rear end of the rod portion and not at the sprue-rod junction (image of the tear position is shown in a later section). The temperature was estimated using the following described method. According to the force curve, the initiation of force drop occurred when the recorded temperatures at TC 1, TC 2,

and TC 3 were 484 ^{0}C, 419 ^{0}C and 398 ^{0}C, respectively. The length of the whole rod was 150 mm. The distance from TC 2 to TC 1 (junction, hot spot) was 75 mm, and distance from TC 3 to TC 1 was 125 mm. The tear was observed at 131 mm away from TC 1. By plotting the temperature against position (distance to the sprue-rod junction), the temperature at the tear location was estimated as 396 ^{0}C. The temperature prediction using the above method was believed to be reasonable in other investigation [12].

As shown in Fig. 5, the final force values for Mg-0.5Ca (348 N, at a time of 1403 s) and Mg-0.5Ca-0.5Zn alloy (460 N, at a time of 1600 s) were significantly higher than those of the other three ternary alloys (all below 160 N, at a time of 1600 s) suggesting that the tear size of Mg-0.5Ca and Mg-0.5Ca-0.5Zn alloys were smaller than that of Mg-0.5Ca-1.5Zn, Mg-0.5Ca-4Zn, and Mg-0.5Ca-6Zn alloys, and that they had the lower HTS. The smaller tear size, the larger force built up observed during cooling. This is because only the tear-free parts contribute to the accumulated contract force. Thus, it is expected that the as-recorded final force can inversely reflect the size of hot tears and consequently the HTS [4]. However, if the final force values of alloys are low and close to each other, this cannot be used to estimate the tear size. For instance, the final forces for Mg-0.5Ca-xZn alloys cast at T_{mould} = 250 ^{0}C were lower than 40 N and quite close to each other, and cannot be used to estimate the tear volume.

3.3 Hot tear evaluation

3.3.1 Macro structure observations

Macro structure images of hot tears in Mg-0.5Ca-xZn alloys at both mould temperatures are shown in Fig. 6. At a mould temperature of 250 ^{0}C, castings of Mg-0.5Ca, Mg-0.5Ca-0.5Zn, Mg-0.5Ca-1.5Zn, and Mg-0.5Ca-4Zn alloys were completely broken. Mg-0.5Ca-6Zn alloy

exhibited multiple tears, which agreed well with the multiple force drops observed on the force-temperature-time curve (Fig. 4 (e)). Among the studied alloys, only Mg-0.5Ca-6Zn alloy did not break suggesting that it had the lowest HTS.

When the mould temperature was 450 ^{0}C, only tiny tears were observed in Mg-0.5Ca and Mg-0.5Ca-0.5Zn alloys, which agreed well with the higher final force values on the force-temperature-time curves (Fig. 5). The severity of hot tears of Mg-0.5Ca, Mg-0.5Ca-0.5Zn, and Mg-0.5Ca-6Zn alloys became less sever in comparison to the tears at a mould temperature of 250 ^{0}C. On the other hand, castings of Mg-0.5Ca-1.5Zn and Mg-0.5Ca-4Zn were completely broken, showing a high HTS even at the higher mould temperature. The hot tear in Mg-0.5Ca-4Zn alloy was observed away from the sprue-rod junction, at the steel screw, as marked in Fig. 6.

Interestingly, small cracks were observed at steel screw for those alloys with hot tears at the sprue-rod junction. These small cracks show that the region was weak and favourable for the hot tearing initiation. Due to the difference in the thermal conductivities between steel (steel screw) and solidifying Mg alloys, stress developed during solidification as the metal and the steel screw contract at different rates resulted in hot tears at this interface. However, the complete fracture observed in Mg-0.5Ca-4Zn alloy at this junction was attributed to the longer freezing range along with slower solidification rate at the higher mould temperature.

The lower solidus temperature (T_s=295 ^{0}C) of Mg-0.5Ca-4Zn alloy and higher mould temperature (450 ^{0}C) increased the time spent by the alloy in the vulnerable temperature region. Normally, the solidification starts from the rear end of the mould, i.e. from the steel screw as the lowest temperature of the molten metal occurred at this point. Then the solidification propagates towards to the sprue-rod junction. Due to the slower cooling and longer freezing range, the stress

initially builds up at the steel screw before it accumulates at the sprue-rod junction. Once the accumulated stress exceeds the strength of the alloy at the interface of the steel screw and solidifying metal, hot tearing occurs. It should be noted that in case of Mg-0.5Ca-4Zn alloy, as the contraction stress was relieved by the complete fracture at the steel screw, the remaining casting solidified freely and no tear appeared at the sprue-rod junction. On the other hand, at a higher solidification rate, the strength builds up quickly at the steel screw due to the faster cooling and hence the contraction stress shifts to the sprue-rod junction. Due to these reasoning, alloys did not break at the steel screw at a mould temperature of 250 ^{0}C.

3.3.2 3D X-ray tomography

3D X-ray tomography is proved to be a useful technique to observe the tear morphology and to evaluate the crack volume quantitatively [7, 8]. Fig. 7 shows the X-ray tomography images of longitudinal cross section at the mid plane of Mg-0.5Ca-6Zn alloy cast at different mould temperatures. Most alloys investigated in this study were broken completely, thus only Mg-0.5Ca-6Zn alloy was analysed with 3D X-ray tomography technique. The cross section of steel tube (TC 1 cover) used for protecting the thermocouple appear as two white lines in the X-ray tomography. The hot tears are indicated by the white arrows. The main tear located away from the exact sprue-rod junction for Mg-0.5Ca-6Zn alloy cast at T_{mould} = 250 ^{0}C whereas it was at the junction at the higher mould temperature. Moreover, Mg-0.5Ca-6Zn alloy showed a severe tear at the lower mould temperature than that at the higher mould temperature. The quantified tear volumes at T_{mould} = 250 ^{0}C and T_{mould} = 450 ^{0}C were 81.73 mm^3 and 48.49 mm^3, respectively.

3.3.3 Tear morphologies

The typical optical microstructures of the longitudinal sections of the Mg-0.5Ca, Mg-0.5Ca-4Zn, and Mg-0.5Ca-6Zn alloys cast at both mould temperatures are shown in Fig. 8. The samples were cut from the regions near the junctions. As the castings at T_{mould} = 250 ^{0}C of Mg-0.5Ca and Mg-0.5Ca-4Zn alloys were completely broken, the tear morphologies in the rod part near the fractured region were observed and are shown in Fig. 8 (a) and (c). Both the sprue and rod parts of Mg-0.5Ca-6Zn alloy were shown in Fig. 8 (e). All the tears propagated mainly along grain boundaries.

Similarly, samples were prepared from the Mg-0.5Ca, Mg-0.5Ca-4Zn, and Mg-0.5Ca-6Zn alloys cast at T_{mould} = 450 ^{0}C and resultant microstructures are shown in Fig. 8 (b), (d), and (f), respectively. Only tiny tears were found at the sprue-rod junction area for Mg-0.5Ca alloy. The grain size of Mg-0.5Ca-4Zn alloy (Fig. 8 (d)) around the tear region (rear end of the rod near the steel screw) was smaller than that at the sprue-rod junction area (Fig. 3 (d)). The tear width of Mg-0.5Ca-6Zn alloy cast at T_{mould} = 450 ^{0}C was smaller than that cast at T_{mould} = 250 ^{0}C, indicating again that higher mould temperature improves the resistance to hot tearing. All the tears observed in the alloys cast at a high mould temperature also propagated along the grain and dendritic boundaries irrespective of their locations along the rod.

SEM photographs of the tear region for Mg-0.5Ca-xZn alloys cast at both mould temperatures are shown in Fig. 9. The amount of second phases increased with the increase in Zn content. Few secondary microcracks were found near the main tear in Mg-0.5Ca-4Zn and Mg-0.5Ca-6Zn alloys cast at T_{mould} = 250 ^{0}C. However, these microcracks were not observed in Mg-0.5Ca, Mg-0.5Ca-0.5Zn, and Mg-0.5Ca-1.5Zn alloys. These microcracks were found mainly at the rod

portion of the junction. Formation of microcracks may decrease the HTS due to the stress relaxation. It was reported that the stress relaxation could also be due to the formation of microposity, which resulted in the reduction of effective tearing strain [33]. The stress relief due to the micro cracks prevented further stress concentration at the junction, thus led to a small primary tear.

Fig. 10 illustrates the microstructures near the tear region of Mg-0.5Ca-xZn alloys cast at T_{mould} = 450 ^{0}C. The microstructures of the alloys were similar to that observed at the low mould temperature of 250 ^{0}C. With the exception of Mg-0.5Ca-4Zn alloys, other alloys did not show any eutectic segregation near the tears.

3.4 Fracture surfaces

At the central regions, typical of hot tearing fracture surfaces were observed in Mg-0.5Ca-xZn alloys cast at T_{mould} = 250 ^{0}C (Fig. 11). The fracture surfaces consisted of mainly dendritic grains and torn liquid films. The amount of torn liquid film was lower in the binary Mg-0.5Ca alloy (Fig. 11 (a)) than that in ternary Mg-Ca-Zn alloys (Fig. 11 (b), (c), (d), and (e)). The micro pores at the central region were only observed in Mg-0.5Ca-4Zn and Mg-0.5Ca-6Zn alloys. This observation agrees well with micro secondary cracks in these alloys shown previously in Fig. 9. The fracture surfaces near the edge region in Mg-0.5Ca-xZn alloys cast at T_{mould} = 250 ^{0}C were similar, but were very different from the central region. The typical fracture surfaces at the edge region are shown in Fig. 12. The torn liquid film was not evident at the edge region, and micro pores between dendrites were observed at the edge region for all the alloys.

The formation of the micro pores at the edge of the rod might be explained as follows. During solidification the heat was removed through mould walls and thus, a small thermal contraction

force may have been generated from the edge to the centre of the rod. This thermal contraction force was much lower than the contraction force along the rod. Due to small contraction force micro pores may form in the edge area.

Fig. 13 shows the fracture surfaces (central region of the rod) of Mg-0.5Ca-1.5Zn and Mg-0.5Ca-4Zn alloys cast at T_{mould} = 450 ^{0}C. No pores were detected in the fracture surfaces obtained from the edges of the rods (microstructures are not shown). Both fracture surfaces show the presence of liquid film confirming that the tear initiated above the solidus temperature. Although tearing in Mg-0.5Ca-4Zn alloy occurred at the interface between alloy and steel screw, the liquid film was still observed. More torn liquid film was observed on fracture surface of Mg-0.5Ca-1.5Zn alloy.

3.5 Effect of Zr addition

The effect of Zr addition on the hot tearing behaviour of Mg-0.5Ca-4Zn alloy is shown in Fig. 14. The addition of Zr decreased the HTS of the alloy at both mould temperatures. At a mould temperature of 250 ^{0}C, the addition of Zr resulted in a wide tear around the rod at the sprue-rod junction but the casting did not completely break. As the mould temperature increased to 450 ^{0}C, no visible tears were observed in the Zr containing alloy at both sprue-rod junction and steel screw region.

The enhancement in hot tearing resistance with the addition of Zr was mainly due to grain refinement. Grain morphologies of alloys cast at a mould temperature of 250 ^{0}C with or without Zr addition are compared in Fig. 15. The grain size was significantly refined with the addition of Zr at both the mould temperatures. The grain size decreased from 126±57 μm to 70±30 μm with the Zr addition at a mould temperature of 250 ^{0}C. At a higher mould temperature of 450 ^{0}C, the

grain size was also refined from 149±74 μm to 64±28 μm for Zr free and Zr containing alloys. Zr is known to be a very efficient grain refiner for Al-free Mg alloys [34-36]. According to solidification calculations using Pandat software, the addition of 0.24 wt.% Zr (actual composition) has little impact on the freezing range (FR) of Mg-0.5Ca-4Zn alloy. The calculated FR of Mg-0.5Ca-4Zn and Mg-0.5Ca-4Zn-0.5Zr were 341 ^{0}C and 342 ^{0}C, respectively. Therefore, only grain refinement was responsible for the decrease in HTS. Improvement in hot tearing resistance, due to grain refinement was reported for Al alloys [37].

4 Discussion

4.1 Effect of Zn addition

The HTS of alloys is affected by the alloy composition as it influences the followings: the susceptible freezing range (ΔT_s, the temperature range of the solid fractions (f_s) between 0.9 and 0.99) and the amount of eutectic liquid (f_{le}, fraction of the eutectic liquid at the eutectic temperature).

Fig. 16 shows the solidification curves of Mg-0.5Ca-xZn alloys calculated with Pandat Software using the Scheil solidification model. The addition of Zn widens the FR of Mg-0.5Ca-xZn alloys. Solidus temperatures of Mg-0.5Ca, Mg-0.5Ca-0.5Zn, and Mg-0.5Ca-x (x= 1.5, 4, and 6) Zn alloys, are at 517 ^{0}C, 394 ^{0}C, and 295 ^{0}C, respectively (Table 3). The susceptible temperature range (ΔT_s) was also calculated and listed in Table 3. It is well established that HTS is extremely sensitive to ΔT_s [38]. When the solid fraction is between 0.9 and 0.99, interdendritic separation occurs. If the remaining liquid is not sufficient to accommodate the interdendritic separation, hot tear forms. Thus, within this temperature range, the casting is most susceptible to hot tearing. In this study, ΔT_s of Mg-0.5Ca-xZn alloys increases with increased Zn content, and reaches a

maximum of 228 ^{0}C for Mg-0.5Ca-4Zn. With further increase in Zn to 6 wt.%, the ΔT_s decreases to 165 ^{0}C.

Both Mg-0.5Ca-1.5Zn and Mg-0.5Ca-4Zn alloys had high HTS, as they were both completely broken even at the high mould temperature (Fig. 6). The tear for Mg-0.5Ca-4Zn alloy even occurred near the rear end of the rod. This reveals that Mg-0.5Ca-4Zn alloy had a higher HTS than Mg-0.5Ca-1.5Zn alloy, as it is much harder for the rod to break away from the sprue-rod junction [5]. Thus, the highest HTS of Mg-0.5Ca-4Zn alloy can be well correlated with the alloy with its largest ΔT_s. A similar correlation between experimental HTS and susceptible temperature range was also established for Mg-Y alloys [7].

The amount of eutectic liquid (f_{le}) also plays an important role in HTS. After hot tears occur, the neighbouring regions have a negative pressure. The negative pressure can suck back the eutectic liquid, and subsequently heal the hot cracks [39]. Liquid healing was reported for Mg-Y and Mg-Gd binary alloys, especially at a high solute content [7, 15]. Generally, the larger f_{le} is present, it is more likely that the solidifying alloy can accommodate the rising tension and heal cracks [11].

The calculated f_{le} of Mg-0.5Ca-xZn- alloys are listed in Table 4. As Mg-0.5Ca, Mg-0.5Ca-4Zn, Mg-0.5Ca-6Zn, and Mg-0.5Ca-4Zn-0.5Zr alloys have a large f_{le}. Normally, a large f_{le} should result in a bulk eutectic which can refill the existing tear. The microstructures near the main tear shown in Fig. 9 (a), (d), (e) and Fig. 17 (a) suggested that the presence of bulk eutectic near the main tear area was only evident in Mg-0.5Ca and Mg-0.5Ca-4Zn-0.5Zr alloys. The above observation suggested that crack refilling by eutectic liquid occurred in these two alloys. Compared with Mg-0.5Ca and Mg-0.5Ca-4Zn-0.5Zr alloys, much less of bulk eutectic was observed in the microstructure of Mg-0.5Ca-4Zn and Mg-0.5Ca-6Zn alloys. The fracture

surfaces of these two alloys (Fig. 11 (d) and (e)) showed a large amount of torn liquid film agglomerates. Such torn liquid film agglomerates were not observed in the fracture surfaces of Mg-0.5Ca (Fig. 11 (a)) and Mg-0.5Ca-4Zn-0.5Zr (Fig. 17 (b)) alloys.

The higher amount of torn liquid film agglomerates and no evidence of bulk eutectic observed in Mg-0.5Ca-4Zn and Mg-0.5Ca-6Zn alloys can be explained as follow. At the later stages of solidification, the residual liquid distributed as a liquid film over the dendrites. With the solidification further proceeding, these liquid films were stretched and finally ruptured under contraction stress [1]. The higher amount of ruptured liquid film (appeared as ruptured liquid film agglomerates on the fracture surface) consumes the residual liquid. Thus, no bulk eutectic formed in Mg-0.5Ca-4Zn and Mg-0.5Ca-6Zn alloys, due to the lack of available residual liquid as a result of the higher consumption of liquid by the ruptured liquid film. In the cases of Mg-0.5Ca and Mg-0.5Ca-4Zn-0.5Zr alloys, small amount of ruptured liquid film consumed only a small amount of residual liquid. Thus the residual liquid could flow into the tear and refill the tear, which appeared as the bulk eutectic near the tear region in the microstructure.

4.2 Effect of grain refinement

The grain refinement of Zr in Al-free Mg alloys is due to the good crystallographic matching between Zr and Mg and the higher growth restriction factor due to the dissolved Zr [36]. α-Zr has a hexagonal crystal structure, and its lattice parameters (a = 0.323 nm, c = 0.514 nm) are very similar to those of Mg (a = 0.321 nm, c = 0.521 nm). Thus, the undissolved zirconium particles can act as effective nucleation sites for magnesium grains [40], which results in grain refinement. Additionally, the dissolved Zr restricts grain growth due to constitutional undercooling which can substantially refine the grain size. Even a small Zr addition is able to

refine the grain size of Mg-3.8Zn-2.2Ca alloy [34]. The present study also suggests that 0.24 wt. % of Zr is able to refine the grain size of Mg-0.5Ca-4Zn alloy.

As both FR and ΔT_s of the alloys with or without Zr were nearly the same (Table 3), the reduced HTS of Mg-0.5Ca-4Zn-0.5Zr is mainly due to grain refinement. Grain refinement delays the onset of strength development and interdendritic feeding, which reduce the HTS [29]. The delayed interdendritic feeding shortens the practical susceptible temperature range of hot tearing. In addition, the refined equiaxed grain microstructure is better for the accommodation of deformation caused by the thermal contraction. With the addition of Zr, lower amount of ruptured liquid film was found on the fracture surface, which was indicative of better compensation. Higher amount of strain can be accommodated by easy slip along the lubricated boundaries with finer grains [41]. Consequently, the hot tearing resistance improves.

4.3 Effect of mould temperature

Hot tearing susceptibility decreased with the increased mould temperature. Due to the extremely high HTS, both Mg-0.5Ca-1.5Zn and Mg-0.5Ca-4Zn alloys still exhibited a high HTS at T_{mould} = 450 ^{0}C. Generally, a high mould temperature improves the hot tearing resistance due to a small thermal gradient and better feeding [42].

During solidification, thermal contraction stresses accumulate due to the thermal gradient. Hot tearing occurs only if the accumulated thermal stresses exceed the critical fracture stress of the casting [43]. Normally, a lower cooling rate induces a small thermal gradient. With a lower cooling rate (high initial mould temperature), the solidification path is close to equilibrium state, which results in a smaller contraction stress and a more homogeneous distribution of solute. Cooling rate in this study is defined as temperature change in the complete solidification range

divided by the corresponding solidification time. Although the cooling conditions, at a same mould temperature were constant, the cooling rates varied from alloy to alloy. The calculated cooling rates of alloys are listed in Table 5. Change in mould temperature did not influence the cooling rates for Mg-0.5Ca-1.5Zn, Mg-0.5Ca-4Zn, Mg-0.5Ca-6Zn, and Mg-0.5Ca-4Zn-0.5Zr alloys, suggesting that the initial mould temperature had a minor effect on the HTS of these alloys (Fig. 6). However, cooling rates of Mg-0.5Ca and Mg-0.5Ca-0.5Zn alloys reduced considerably when the mould temperature increased, which is consistent with the reduced HTS at higher mould temperature (Fig. 6).

In addition, total solidification time increased with increase in initial mould temperature. Hence a higher initial mould temperature provides better compensation of stress and strains. Generally, the accumulated contraction strain can be eliminated or reduced through microscopic movements of the dendrite cells or liquid metal, which is regarded as compensation. The long duration of solidification provides adequate time to compensate the strain developed. However, the time for compensation may not be sufficient at a fast solidification process (low initial mould temperature).

5 Conclusions

Effect of Zn addition on hot tearing behaviour of Mg-0.5Ca alloys was investigated and the hot tearing mechanism was discussed. The conclusions are summarized as follows:

1. Mg-0.5Ca-xZn (x=0, 0.5, 1.5, 4, and 6) alloys exhibited a high hot tearing susceptibility. However, the addition of 6 wt.% Zn improved the hot tearing resistance of Mg-0.5Ca-xZn alloys.

2. Hot tears were mostly observed at the sprue-rod junction. However, hot tears of Mg-0.5Ca-4Zn cast at T_{mould} = 450 ^{0}C appeared at the rear side of the rod portion near the steel screw suggested its high HTS.
3. The secondary micro cracks were found in the centre of sprue-rod junction for Mg-0.5Ca-4Zn and Mg-0.5Ca-6Zn alloys cast at T_{mould} = 250 ^{0}C. The formation of these micro cracks resulted in stress relaxation, which might alleviate the hot tearing.
4. The susceptible freezing range (ΔT_s) as well as amount of eutectic liquid (f_{le}) change with respect to the amount of Zn content in Mg-0.5Ca alloy. A good correlation between ΔT_s and HTS of Mg-0.5Ca-xZn alloys was established: high ΔT_s leads to higher HTS. The residual liquid might form either liquid film agglomerates or bulk eutectic near the hot tears. Only the bulk eutectic was found beneficial for the low HTS.
5. The high initial mould temperature decreased HTS of alloys, with the exception of Mg-0.5Ca-1.5Zn and Mg-0.5Ca-4Zn alloys. The higher initial mould temperature led to the small thermal gradient, which resulted in the improved hot tearing resistance.
6. Grain refinement with addition of Zr to Mg-0.5Ca-4Zn alloy decreased the HTS at both mould temperatures as it delayed the onset of strength development, interdendritic feeding, as well as enhanced accommodation of strain developed during solidification.

Acknowledgements

The authors would like to thank Mrs. Petra Fischer, Mr. Guenter Meister, Mr. Gert Wiese for their technical support and Dr. Chamini Mendis for her English corrections. Financial support from China Scholarship Council (CSC) for this work is greatly appreciated.

References

[1] Katgerman L, Eskin DG. In search of the prediction of hot cracking in aluminium alloys. Hot Cracking Phenomena in Welds II. Berlin: Springer Berlin Heidelberg; 2008. p. 11-26.

[2] Zhen ZS, Hort N, Huang YD, Utke O, Petri N, Kainer KU. Hot tearing behaviour of binary Mg–1Al alloy using a contraction force measuring method. Int J Cast Metal Res. 2009;22:331-4.

[3] Cao G, Zhang C, Cao H, Chang YA, Kou S. Hot-Tearing Susceptibility of Ternary Mg-Al-Sr Alloy Castings. Metall and Mat Trans A. 2010;41:706-16.

[4] Zhen Z, Hort N, Huang Y, Petri N, Utke O, Kainer KU. Quantitative Determination on Hot Tearing in Mg-Al Binary Alloys. Mater Sci Forum. 2009;618-619:533-40.

[5] Cao G, Kou S. Hot cracking of binary Mg–Al alloy castings. Materials Science and Engineering: A. 2006;417:230-8.

[6] Zhou L, Huang YD, Mao PL, Kainer KU, Liu Z, Hort N. Influence of composition on hot tearing in binary Mg–Zn alloys. Int J Cast Metal Res. 2011;24:170-6.

[7] Wang Z, Huang Y, Srinivasan A, Liu Z, Beckmann F, Kainer KU, et al. Hot tearing susceptibility of binary Mg–Y alloy castings. Mater Design. 2013;47:90-100.

[8] Srinivasan A, Wang Z, Huang Y, Beckmann F, Kainer K, Hort N. Hot Tearing Characteristics of Binary Mg-Gd Alloy Castings. Metall and Mat Trans A. 2013;44:2285-98.

[9] Wang Z, Huang YD, Srinivasan A, Liu Z, Kainer KU, Hort N. Influences of Y Additions on the Hot Tearing Susceptibility of Mg-1.5wt.%Zn Alloys. Mater Sci Forum. 2013;765:306-10.

[10] Gunde P, Schiffl A, Uggowitzer PJ. Influence of yttrium additions on the hot tearing susceptibility of magnesium–zinc alloys. Materials Science and Engineering: A. 2010;527:7074-9.

[11] CAO G, KOU S. Hot tearing of ternary Mg-Al-Ca alloy castings. Metall and Mat Trans A. 2006;37A:3647-63.

[12] Cao G, Haygood I, Kou S. Onset of Hot Tearing in Ternary Mg-Al-Sr Alloy Castings. Metall and Mat Trans A. 2010;41:2139-50.

[13] Zhou L, Huang YD, Mao PL, Kainer KU, Liu Z, Hort N. Investigations on Hot Tearing of Mg-Zn-(Al) Alloys. In: Sillekens WH, Agnew SR, Neelameggham NR, Mathaudhu SN, editors.: John Wiley & Sons; 2011. p. 125-30.

[14] Wang Y, Wang Q, Wu G, Zhu Y, Ding W. Hot-tearing susceptibility of Mg–9Al–xZn alloy. Mater Lett. 2002;57:929-34.

[15] Srinivasan A, Wang Z, Huang YD, Beckmann F, Kainer KU, Hort N. Hot Tearing Susceptibility of Magnesium-Gadolinium Binary Alloys. T Indian I Metals. 2012;65:701-6.

[16] Wang Z, Huang Y, Srinivasan A, Liu Z, Beckmann F, Kainer K, et al. Experimental and numerical analysis of hot tearing susceptibility for Mg–Y alloys. J Mater Sci. 2014;49:353-62.

[17] Wang Z, Song J, Huang Y, Srinivasan A, Liu Z, Kainer K, et al. An Investigation on Hot Tearing of Mg-4.5Zn-(0.5Zr) Alloys with Y Additions. Metall and Mat Trans A. 2015;46:2108-18.

[18] Zhang B, Hou Y, Wang X, Wang Y, Geng L. Mechanical properties, degradation performance and cytotoxicity of Mg–Zn–Ca biomedical alloys with different compositions. Materials Science and Engineering: C. 2011;31:1667-73.

[19] B.P.Zhang, Y.Wang, L.Geng. Research on Mg-Zn-Ca Alloy as Degradable Biomaterial. In: Pignatello R, editor. Biomaterials - Physics and Chemistry: InTech; 2011. p. 183-204.

[20] Sun Y, Zhang B, Wang Y, Geng L, Jiao X. Preparation and characterization of a new biomedical Mg–Zn–Ca alloy. Mater Design. 2012;34:58-64.

[21] Gao X, Zhu SM, Muddle BC, Nie JF. Precipitation-hardened Mg–Ca–Zn alloys with superior creep resistance. Scripta Mater. 2005;53:1321-6.

[22] Tong LB, Zheng MY, Hu XS, Wu K, Xu SW, Kamado S, et al. Influence of ECAP routes on microstructure and mechanical properties of Mg–Zn–Ca alloy. Materials Science and Engineering: A. 2010;527:4250-6.

[23] Zhang B, Wang Y, Geng L, Lu C. Effects of calcium on texture and mechanical properties of hot-extruded Mg–Zn–Ca alloys. Materials Science and Engineering: A. 2012;539:56-60.

[24] Tong LB, Zheng MY, Chang H, Hu XS, Wu K, Xu SW, et al. Microstructure and mechanical properties of Mg–Zn–Ca alloy processed by equal channel angular pressing. Materials Science and Engineering: A. 2009;523:289-94.

[25] Fang DQ, Li XJ, Li H, Peng QM. Electrochemical Corrosion Behavior of Backward Extruded Mg-Zn-Ca Alloys in Different Media. International Journal of Electrochemical Science. 2013;8:2551-65.

[26] Somekawa H, Mukai T. High strength and fracture toughness balance on the extruded Mg–Ca–Zn alloy. Materials Science and Engineering: A. 2007;459:366-70.

[27] Tong LB, Zheng MY, Xu SW, Kamado S, Du YZ, Hu XS, et al. Effect of Mn addition on microstructure, texture and mechanical properties of Mg–Zn–Ca alloy. Materials Science and Engineering: A. 2011;528:3741-7.

[28] Gao JH, Guan SK, Ren ZW, Sun YF, Zhu SJ, Wang B. Homogeneous corrosion of high pressure torsion treated Mg–Zn–Ca alloy in simulated body fluid. Mater Lett. 2011;65:691-3.

[29] Easton M, Grandfield J, StJohn D, Rinderer B. The effect of grain refinement and cooling rate on the hot tearing of wrought aluminium alloys. Mater Sci Forum. 2006;519-521:1675-80.

[30] Easton M, Wang H, Grandfield J, StJohn D, Sweet E. An analysis of the effect of grain refinement on the hot tearing of aluminium alloys. Materials Forum. 2004;28:224-9.

[31] Zhen Z, Hort N, Utke O, Huang Y, Petri N, Kainer KU. Investigations on hot tearing of Mg-Al binary alloys by using a new quantitative method. In: Nyberg EA, Agnew SR, Neelameggham NR, Pekguleryuz MO, editors. TMS Wiley; 2009. p. 105-10.

[32] D'Elia F, Ravindran C, Sediako D, Kainer KU, Hort N. Hot tearing mechanisms of B206 aluminum–copper alloy. Mater Design. 2014;64:44-55.

[33] M'Hamdi M, Mo A, Fjær H. TearSim: A two-phase model addressing hot tearing formation during aluminum direct chill casting. Metall and Mat Trans A. 2006;37:3069-83.

[34] Qian M, Das A. Grain refinement of magnesium alloys by zirconium: Formation of equiaxed grains. Scripta Mater. 2006;54:881-6.

[35] Sun M, Easton MA, StJohn DH, Wu GH, Abbott TB, Ding WJ. Grain Refinement of Magnesium Alloys by Mg-Zr Master Alloys: The Role of Alloy Chemistry and Zr Particle Number Density. Adv Eng Mater. 2013;15:373-8.

[36] Stjohn DH, Easton MA, Qian M, Taylor JA. Grain Refinement of Magnesium Alloys: A Review of Recent Research, Theoretical Developments, and Their Application. Metallurgical and Materials Transactions a-Physical Metallurgy and Materials Science. 2013;44A:2935-49.

[37] Lin S, Aliravci C, Pekguleryuz MO. Hot-Tear Susceptibility of Aluminum Wrought Alloys and the Effect of Grain Refining. Metall and Mat Trans A. 2007;38:1056-68.

[38] Clyne TW, G.J.Davies. Comparison between experimental data and theoretical predictions relating to dependence of solidification cracking on composition. Solidification and casting of metals. London: Metals society; 1979. p. 274-8.

[39] Huang YD, Wang Z, Srinivasan A, Kainer KU, Hort N. Metallurgical Characterization of Hot Tearing Curves Recorded during Solidification of Magnesium Alloys. Acta Phys Pol A. 2012;122:497-500.

[40] Song CJ, Han QY, Zhai QJ. Review of grain refinement methods for as-cast microstructure of magnesium alloy. China Foundry. 2009;6:93-103.

[41] Campbell J. Casting. Second ed. Great Britain: Elsevier Science Ltd.; 2003.

[42] Huang H, Fu P-h, Wang Y-x, Peng L-m, Jiang H-y. Effect of pouring and mold temperatures on hot tearing susceptibility of AZ91D and Mg–3Nd–0.2Zn–Zr Mg alloys. T Nonferr Metal Soc. 2014;24:922-9.

[43] Eskin DG, Suyitno, Katgerman L. Mechanical properties in the semi-solid state and hot tearing of aluminium alloys. Prog Mater Sci. 2004;49:629-711.

Table captions

Table 1. Actual chemical compositions of the cast alloys (wt.%).

Table 2. Grain sizes of Mg-0.5Ca-xZn alloys at both mould temperatures

Table 3. Calculated temperatures (in ^{0}C) at different solid fractions with Scheil model of Mg-0.5Ca-xZn-(0.5Zr) alloys, T_l: liquidus temperature, T_s: solidus temperature, FR: freezing range, $T_{0.9}$: temperature at fs=0.9, $T_{0.99}$: temperature at fs=0.99, ΔT_s: $T_{0.9}$-$T_{0.99}$.

Table 4. Fractions of eutectic liquid in Mg-0.5Ca-xZn-(0.5Zr) alloys.

Table 5. Calculated cooling rates of alloys cast at different mould temperatures.

Figure captions

Fig. 1. (a) Schematic of CRC mould and casting, (b) experimental casting, (TC-thermocouple).

Fig. 2. Sample for 3D X-ray tomography observation.

Fig. 3. Optical microstructures of alloys cast at T_{mould} = 250 ^{0}C, (a) Mg-0.5Ca, (c) Mg-0.5Ca-4Zn, (e) Mg-0.5Ca-6Zn, and alloys cast at T_{mould} = 450 ^{0}C, (b) Mg-0.5Ca, (d) Mg-0.5Ca-4Zn, (f) Mg-0.5Ca-6Zn.

Fig. 4. Overall force-temperature-time curves of alloys cast at T_{mould} = 250 ^{0}C, (a) Mg-0.5Ca, (b) Mg-0.5Ca-0.5Zn, (c) Mg-0.5Ca-1.5Zn, (d) Mg-0.5Ca-4Zn, (e) Mg-0.5Ca-6Zn, and (f) typical determination of hot tearing initiation in Mg-0.5Ca-4Zn.

Fig. 5. Force-temperature-time curves of alloys cast at T_{mould} = 450 ^{0}C, (a) Mg-0.5Ca, (b) Mg-0.5Ca-0.5Zn, (c) Mg-0.5Ca-1.5Zn, (d) Mg-0.5Ca-4Zn, and (e) Mg-0.5Ca-6Zn.

Fig. 6. Macro photographs of the hot tears for Mg-0.5Ca-xZn alloys cast at T_{mould} = 250 ^{0}C and T_{mould} = 450 ^{0}C.

Fig. 7. 3D X-ray tomography photographs of Mg-0.5Ca-6Zn alloy cast at different mould temperatures, (a) T_{mould} = 250 ^{0}C, (b) T_{mould} = 450 ^{0}C.

Fig. 8. Optical microstructures showing the tearing paths for the alloys cast at T_{mould} = 250 ^{0}C, (a) Mg-0.5Ca, (c) Mg-0.5Ca-4Zn, (e) Mg-0.5Ca-6Zn, and alloys cast at T_{mould} = 450 ^{0}C, (b) Mg-0.5Ca, (d) Mg-0.5Ca-4Zn, (f) Mg-0.5Ca-6Zn.

Fig. 9. Microstructures near the tear region for the alloys cast at T_{mould} = 250 ^{0}C, (a) Mg-0.5Ca, (b) Mg-0.5Ca-0.5Zn, (c) Mg-0.5Ca-1.5Zn, (d) Mg-0.5Ca-4Zn, and (e) Mg-0.5Ca-6Zn.

Fig. 10. Microstructures near the tear region of alloys cast at T_{mould} = 450 ^{0}C, (a) Mg-0.5Ca, (b) Mg-0.5Ca-0.5Zn, (c) Mg-0.5Ca-1.5Zn, (d) Mg-0.5Ca-4Zn, and (e) Mg-0.5Ca-6Zn.

Fig. 11. Fracture surfaces at the centre region of Mg-0.5Ca-xZn alloys cast at T_{mould} = 250 ^{0}C, (a) Mg-0.5Ca, (b) Mg-0.5Ca-0.5Zn, (c) Mg-0.5Ca-1.5Zn, (d) Mg-0.5Ca-4Zn, and (e) Mg-0.5Ca-6Zn

Fig. 12. Typical fracture surfaces at the edge region of Mg-0.5Ca-xZn alloys cast at T_{mould} = 250 ^{0}C, (a) Mg-0.5Ca, (b) Mg-0.5Ca-4Zn.

Fig. 13. Fracture surfaces of alloys cast at T_{mould} = 450 ^{0}C, (a) Mg-0.5Ca-1.5Zn, and (b) Mg-0.5Ca-4Zn.

Fig. 14. Macro photographs of the hot tears for Mg-0.5Ca-4Zn and Mg-0.5Ca-4Zn-0.5Zr alloys cast at both mould temperatures.

Fig. 15. Grain structures at the sprue-rod junction for alloys cast at a mould temperature of 250 ^{0}C, (a) Mg-0.5Ca-4Zn, (b) Mg-0.5Ca-4Zn-0.5Zr

Fig. 16. Solid fraction as a function of temperature for Mg-0.5Ca-xZn alloys calculated with Pandat Software.

Fig. 17. (a) Microstructure of the cross sections, (b) fracture surface of hot tears for Mg-0.5Ca-4Zn-0.5Zr alloys cast at T_{mould} = 250 ^{0}C.

Table 1

Table 1. Actual chemical compositions of the cast alloys (wt.%).

Alloys	Ca	Zn	Zr	Fe	Mn	Si	Mg
Mg-0.5Ca	0.53	-	-	0.0037	0.0383	0.0108	Bal.
Mg-0.5Ca-0.5Zn	0.44	0.42	-	0.0044	0.0394	0.0145	Bal.
Mg-0.5Ca-1.5Zn	0.43	1.43	-	0.0050	0.0380	0.0167	Bal.
Mg-0.5Ca-4Zn	0.39	4.13	-	0.0051	0.0353	0.0179	Bal.
Mg-0.5Ca-6Zn	0.38	6.20	-	0.0063	0.0387	0.0164	Bal.
Mg-0.5Ca-4Zn-0.5Zr	0.42	3.84	0.24	0.0029	0.0384	0.0055	Bal.

Table 2

Table 2 Grain sizes of Mg-0.5Ca-xZn alloys at both mould temperatures.

Alloys	**T_{mould} = 250 ^{o}C (µm)**	**T_{mould} = 450 ^{o}C (µm)**
Mg-0.5Ca	323±291	475±272
Mg-0.5Ca-0.5Zn	228±145	356±247
Mg-0.5Ca-1.5Zn	136±82	307±165
Mg-0.5Ca-4Zn	126±57	149±74
Mg-0.5Ca-6Zn	125±57	176±88

Table 3

Table 3.Calculated temperatures (in ^{0}C) at different solid fractions with Scheil model of Mg-0.5Ca-xZn-(0.5Zr) alloys, T_l: liquidus temperature, T_s: solidus temperature, FR: freezing range, $T_{0.9}$: temperature at fs=0.9, $T_{0.99}$: temperature at fs=0.99, ΔT_s: $T_{0.9}$-$T_{0.99}$.

	Mg-0.5Ca	**Mg-0.5Ca-0.5Zn**	**Mg-0.5Ca-1.5Zn**	**Mg-0.5Ca-4Zn**	**Mg-0.5Ca-6Zn**	**Mg-0.5Ca-4Zn-0.5Zr**
T_l	647	646	643	636	629	637
T_s	517	394	295	295	295	295
FR	130	252	348	341	334	342
$T_{0.9}$	622	611	589	523	460	523
$T_{0.99}$	517	415	394	295	295	295
ΔT_s	105	196	195	228	165	228

Table 4

Table 4. Fractions of eutectic liquid in Mg-0.5Ca-xZn-(0.5Zr) alloys.

Alloys	**Mg-0.5Ca**	**Mg-0.5Ca-0.5Zn**	**Mg-0.5Ca-1.5Zn**	**Mg-0.5Ca-4Zn**	**Mg-0.5Ca-6Zn**	**Mg-0.5Ca-4Zn-0.5Zr**
$\mathbf{f_{le}}$	0.027	0.008	0.0001	0.032	0.058	0.032

Table 5

Table 5. Calculated cooling rates of alloys cast at different mould temperatures.

Cooling rates(^{0}C/s)	**Mg-0.5Ca**	**Mg-0.5Ca-0.5Zn**	**Mg-0.5Ca-1.5Zn**	**Mg-0.5Ca-4Zn**	**Mg-0.5Ca-6Zn**	**Mg-0.5Ca-4Zn-0.5Zr**
T_{mould} =250 ^{0}C	4.25±0.28	0.56±0.04	0.27±0.02	0.27±0.02	0.26 ±0.01	0.25±0.01
T_{mould} =450 ^{0}C	0.44±0.03	0.22±0.01	0.17±0.01	0.18±0.01	0.17±0.01	0.15±0.01

Figure 1

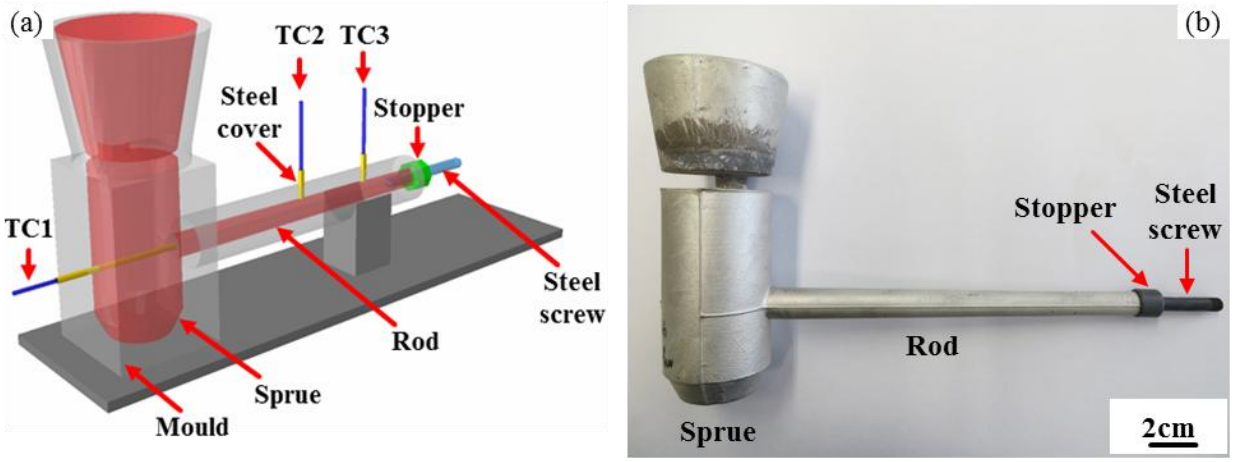

Fig. 1. (a) Schematic of CRC mould and casting, (b) experimental casting, (TC-thermocouple).

Figure 2

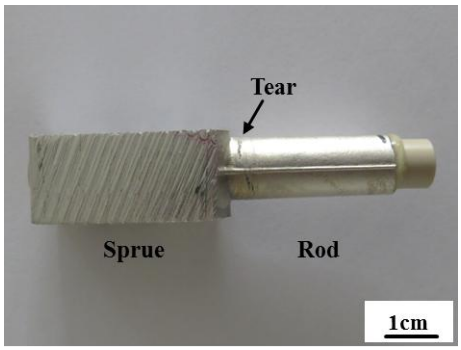

Fig. 2. Sample for 3D X-ray tomography observation.

Figure 3

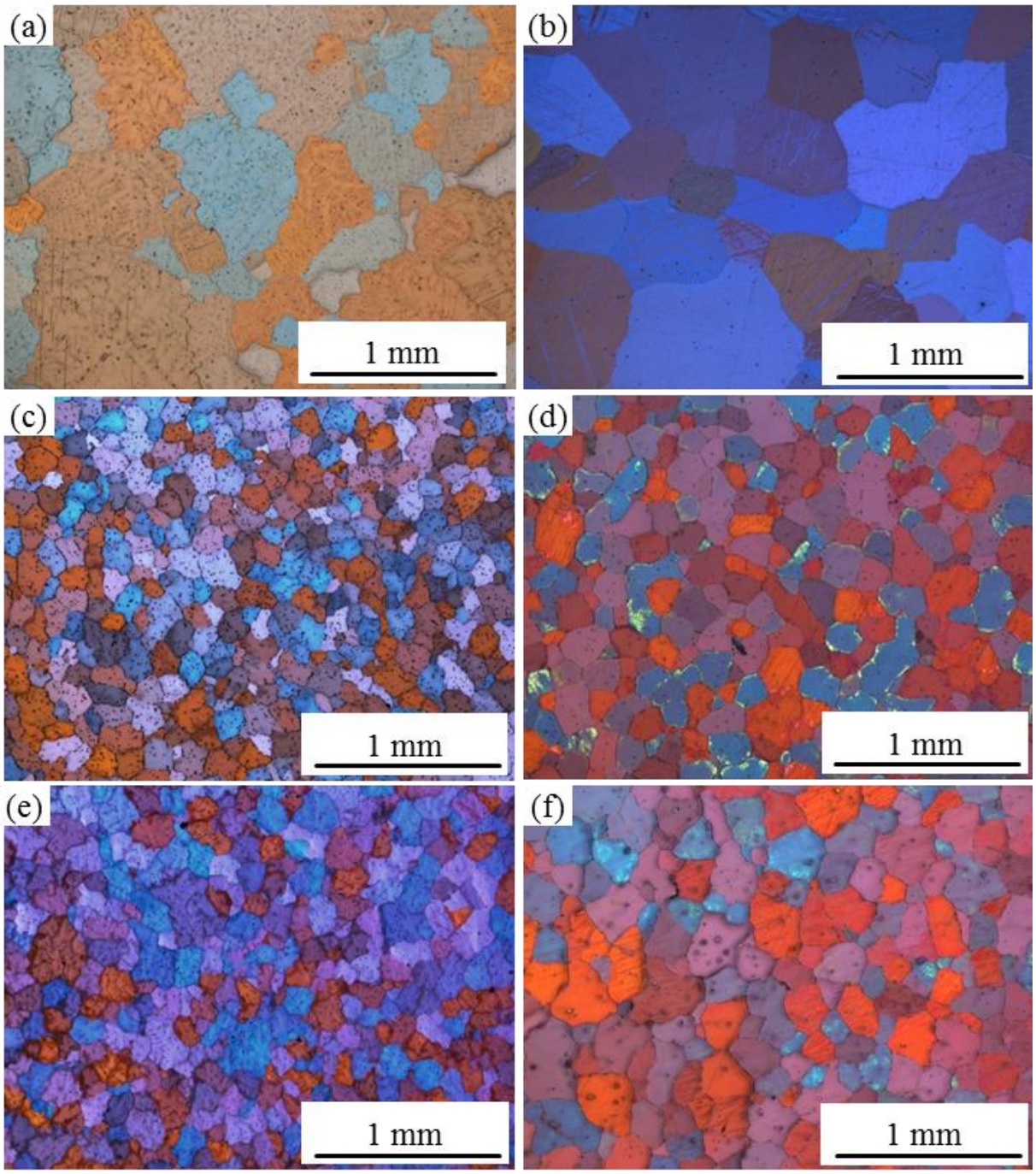

Fig. 3. Optical microstructures of alloys cast at T_{mould} = 250 ^{0}C, (a) Mg-0.5Ca, (c) Mg-0.5Ca-4Zn, (e) Mg-0.5Ca-6Zn, and alloys cast at T_{mould} = 450 ^{0}C, (b) Mg-0.5Ca, (d) Mg-0.5Ca-4Zn, (f) Mg-0.5Ca-6Zn.

Figure 4

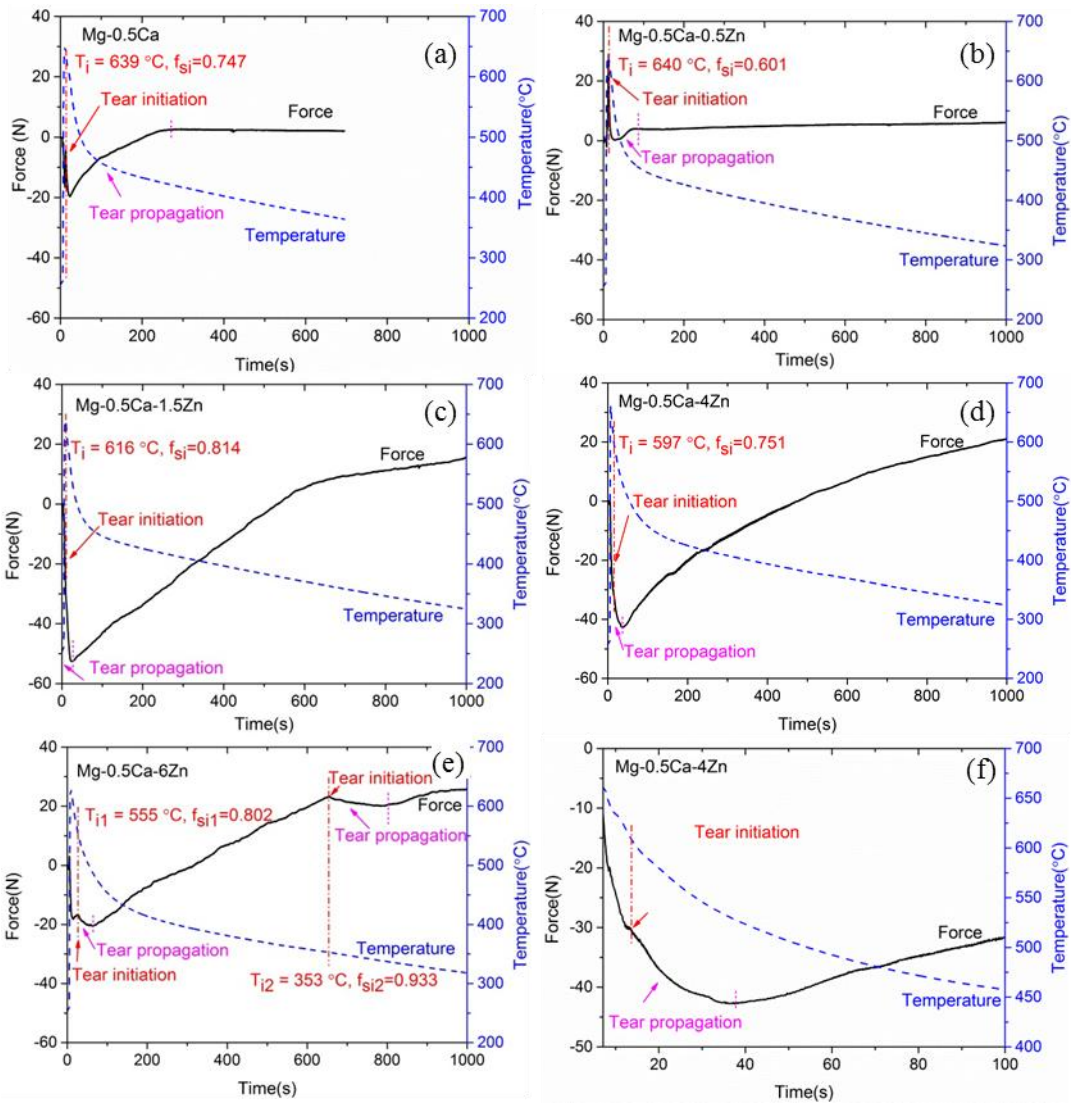

Fig. 4. Overall force-temperature-time curves of alloys cast at T_{mould} = 250 ^{0}C, (a) Mg-0.5Ca, (b) Mg-0.5Ca-0.5Zn, (c) Mg-0.5Ca-1.5Zn, (d) Mg-0.5Ca-4Zn, (e) Mg-0.5Ca-6Zn, and (f) typical determination of hot tearing initiation in Mg-0.5Ca-4Zn.

Figure 5

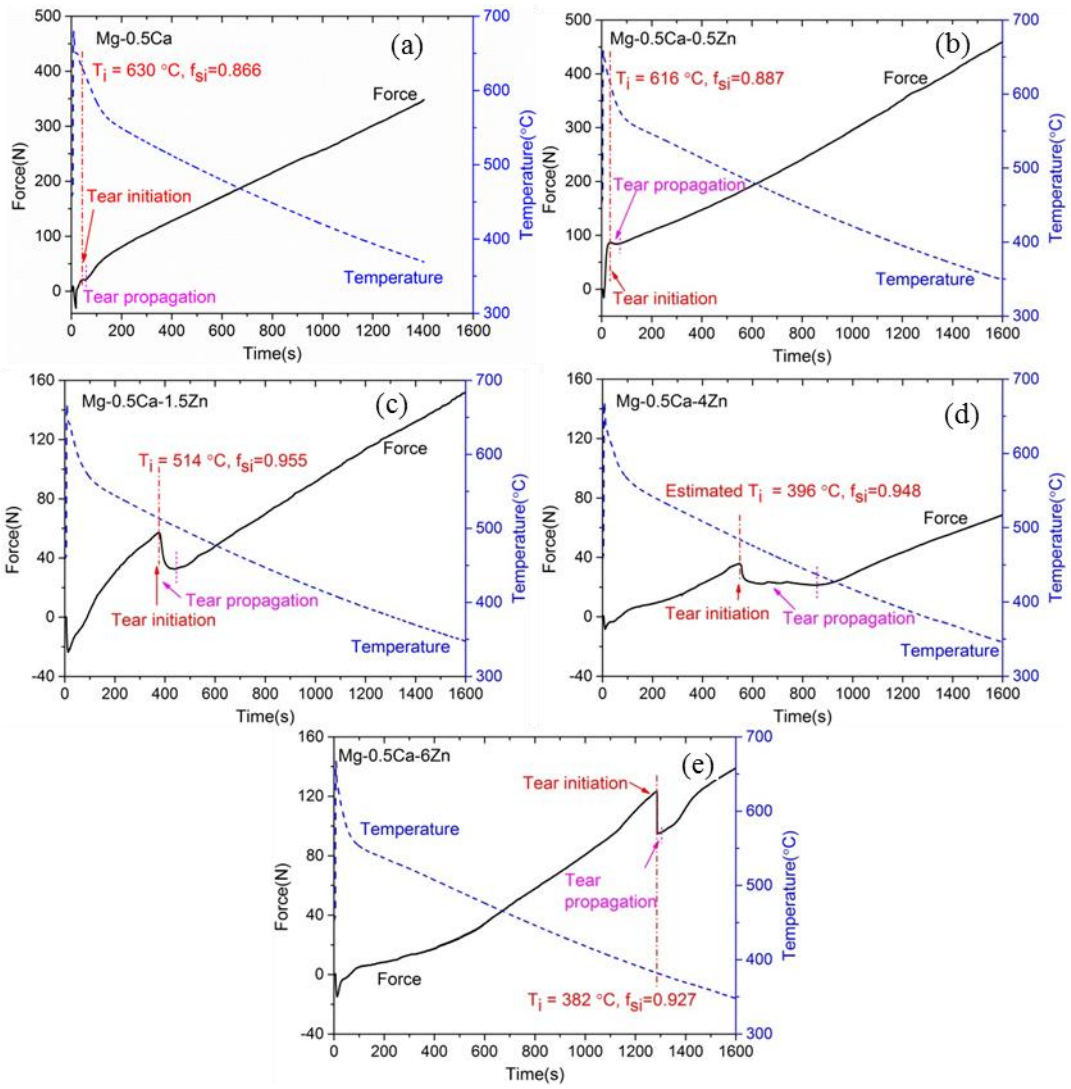

Fig. 5. Force-temperature-time curves of alloys cast at T_{mould} = 450 ^{0}C, (a) Mg-0.5Ca, (b) Mg-0.5Ca-0.5Zn, (c) Mg-0.5Ca-1.5Zn, (d) Mg-0.5Ca-4Zn, and (e) Mg-0.5Ca-6Zn.

Figure 6

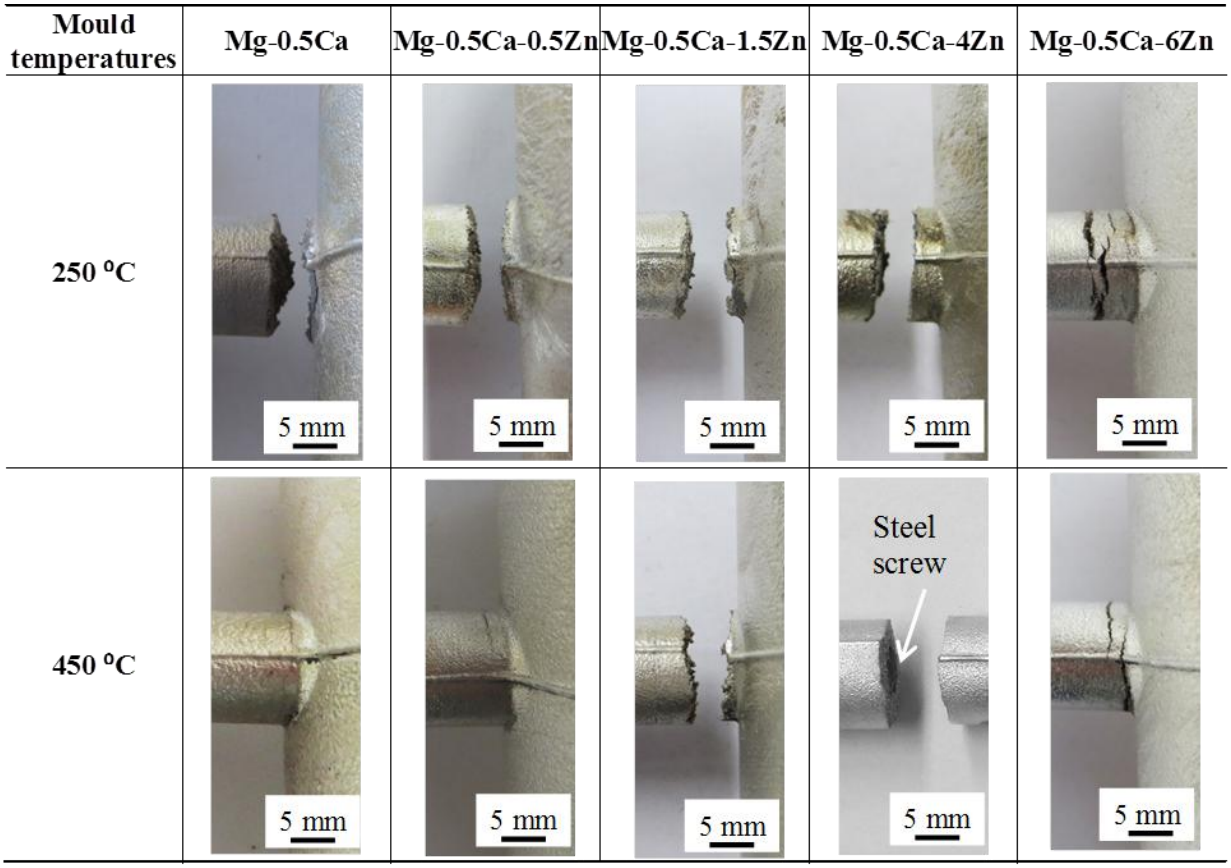

Fig. 6. Macro photographs of the hot tears for Mg-0.5Ca-xZn alloys cast at T_{mould} = 250 ^{0}C and T_{mould} = 450 ^{0}C.

Figure 7

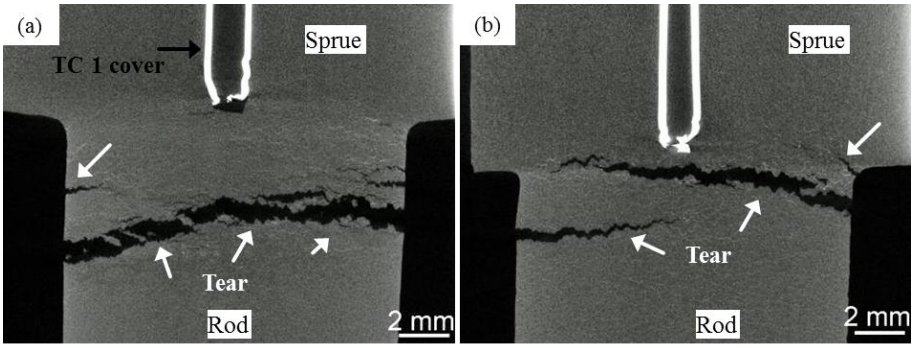

Fig. 7. 3D X-ray tomography photographs of Mg-0.5Ca-6Zn alloy cast at different mould temperatures, (a) T_{mould} = 250 ^{0}C, (b) T_{mould} = 450 ^{0}C.

Figure 8

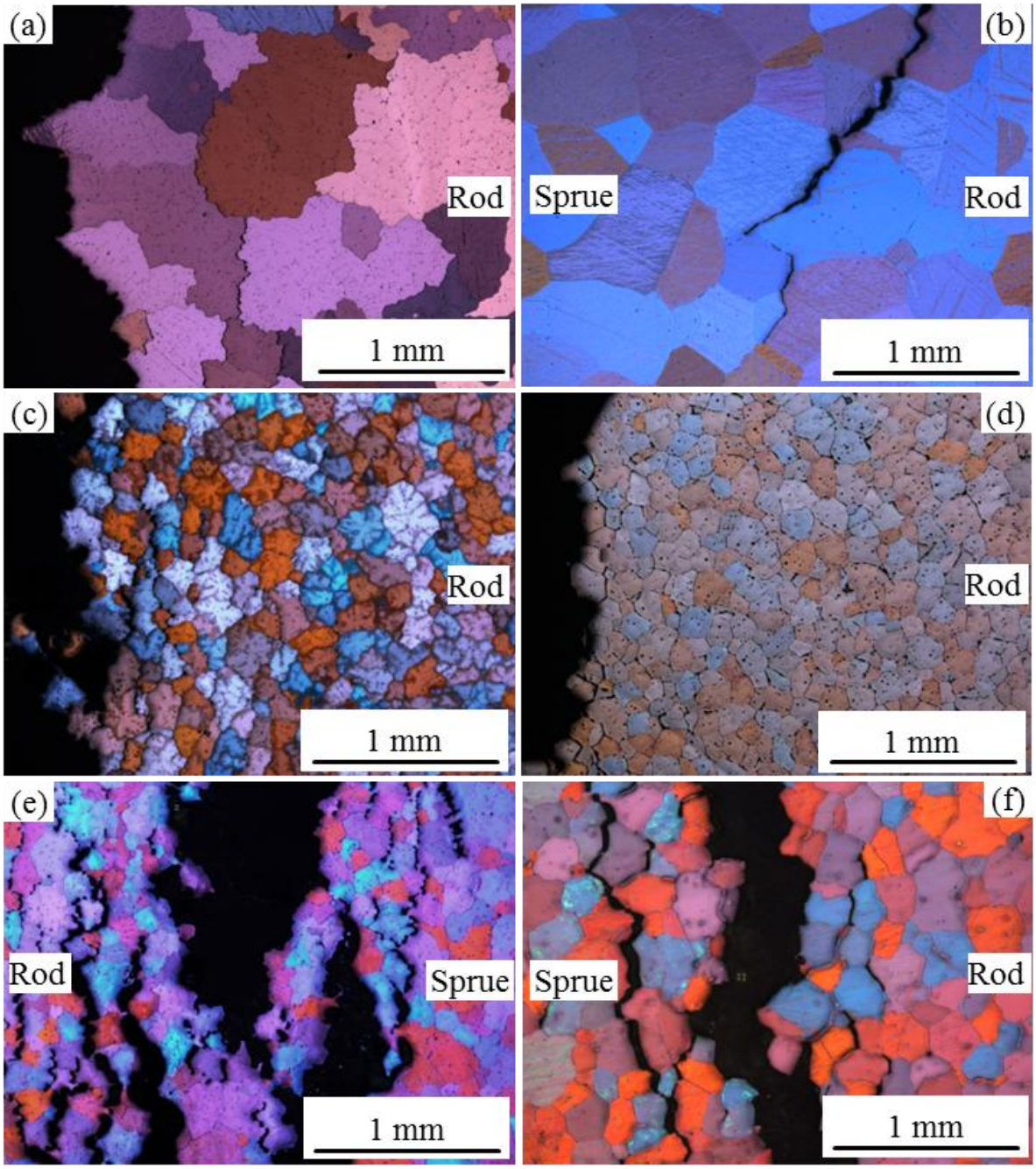

Fig. 8. Optical microstructures showing the tearing paths for the alloys cast at T_{mould} = 250 ^{0}C, (a) Mg-0.5Ca, (c) Mg-0.5Ca-4Zn, (e) Mg-0.5Ca-6Zn, and alloys cast at T_{mould} = 450 ^{0}C, (b) Mg-0.5Ca, (d) Mg-0.5Ca-4Zn, (f) Mg-0.5Ca-6Zn.

Figure 9

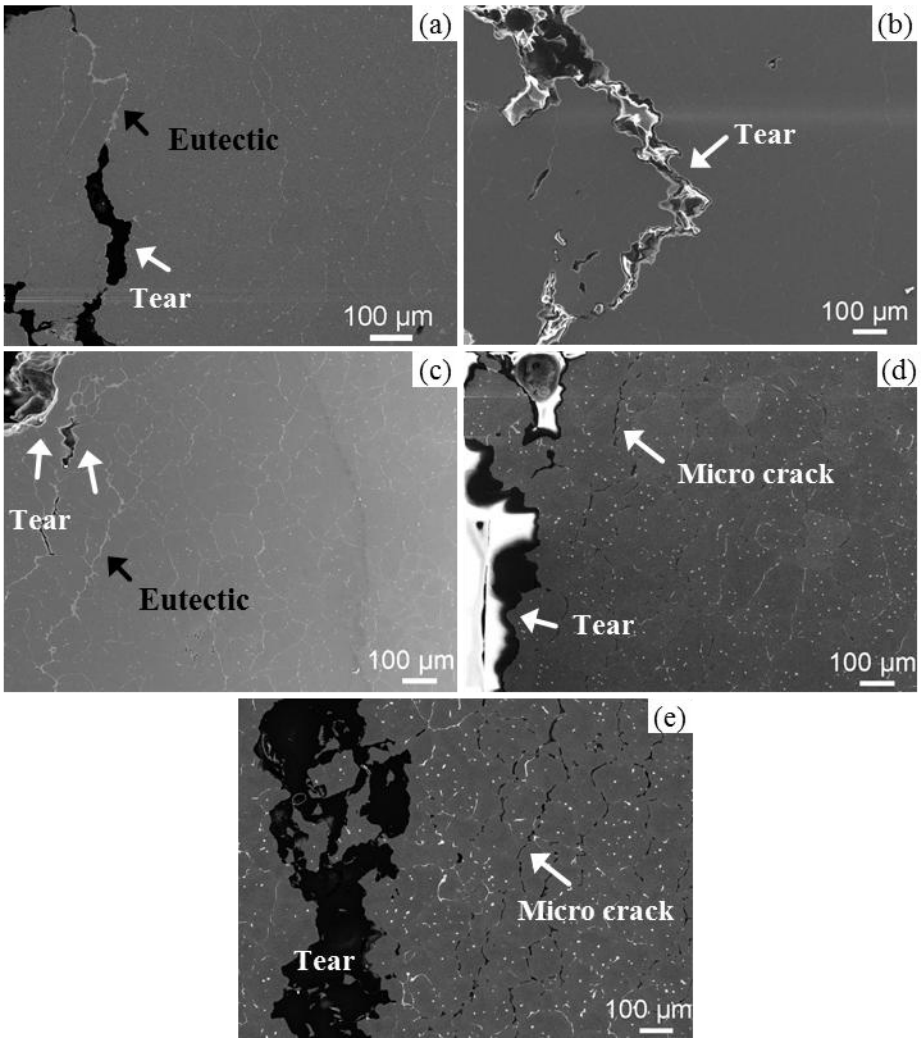

Fig. 9. Microstructures near the tear region for the alloys cast at T_{mould} = 250 ^{0}C, (a) Mg-0.5Ca, (b) Mg-0.5Ca-0.5Zn, (c) Mg-0.5Ca-1.5Zn, (d) Mg-0.5Ca-4Zn, and (e) Mg-0.5Ca-6Zn.

Figure 10

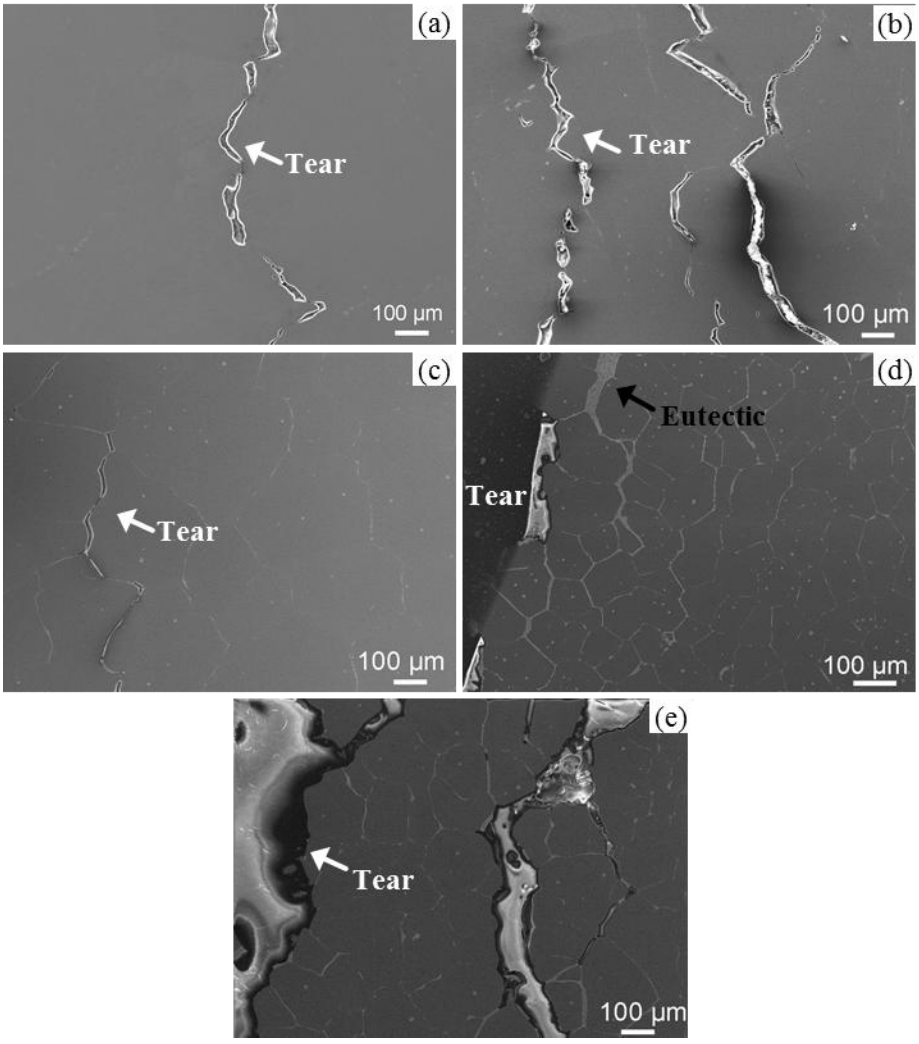

Fig. 10. Microstructures near the tear region of alloys cast at T_{mould} = 450 ^{0}C, (a) Mg-0.5Ca, (b) Mg-0.5Ca-0.5Zn, (c) Mg-0.5Ca-1.5Zn, (d) Mg-0.5Ca-4Zn, and (e) Mg-0.5Ca-6Zn.

Figure 11

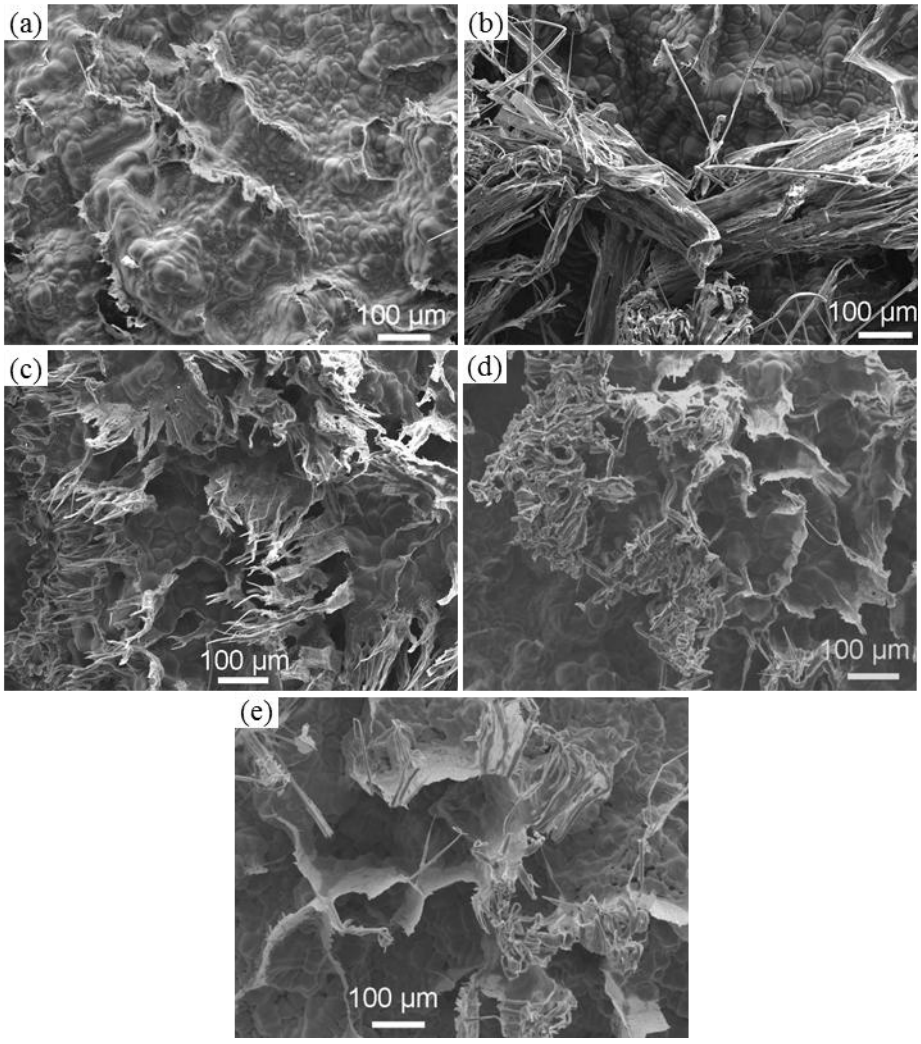

Fig. 11. Fracture surfaces at the centre region of Mg-0.5Ca-xZn alloys cast at T_{mould} = 250 ^{0}C, (a) Mg-0.5Ca, (b) Mg-0.5Ca-0.5Zn, (c) Mg-0.5Ca-1.5Zn, (d) Mg-0.5Ca-4Zn, and (e) Mg-0.5Ca-6Zn.

Figure 12

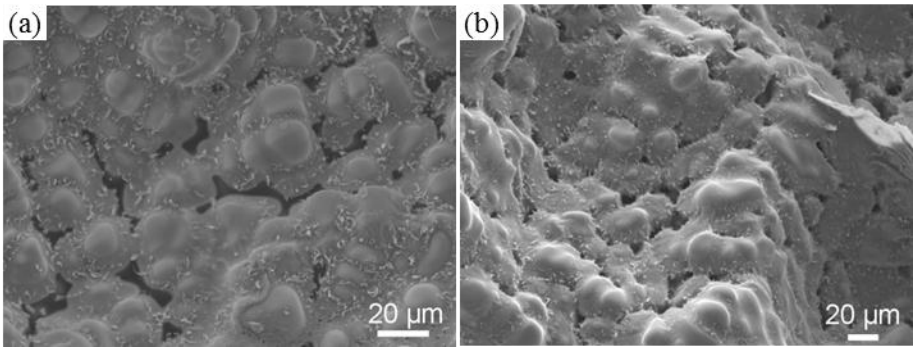

Fig. 12 Typical fracture surfaces at the edge region of Mg-0.5Ca-xZn alloys cast at T_{mould} = 250 ^{0}C, (a) Mg-0.5Ca, (b) Mg-0.5Ca-4Zn.

Figure 13

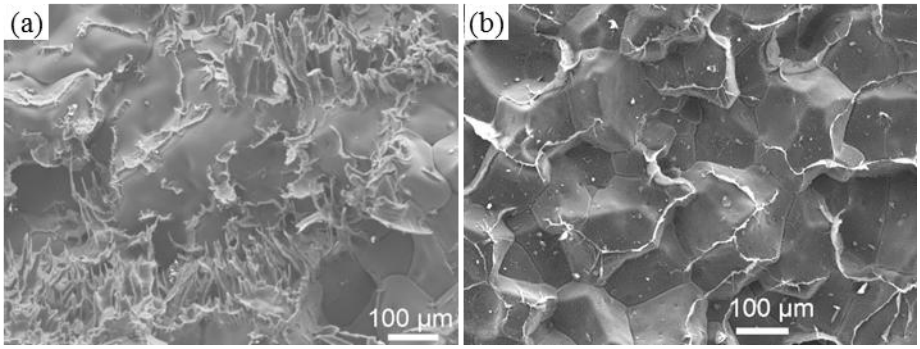

Fig. 13. Fracture surfaces of alloys cast at T_{mould} = 450 ^{0}C, (a) Mg-0.5Ca-1.5Zn, and (b) Mg-0.5Ca-4Zn.

Figure 14

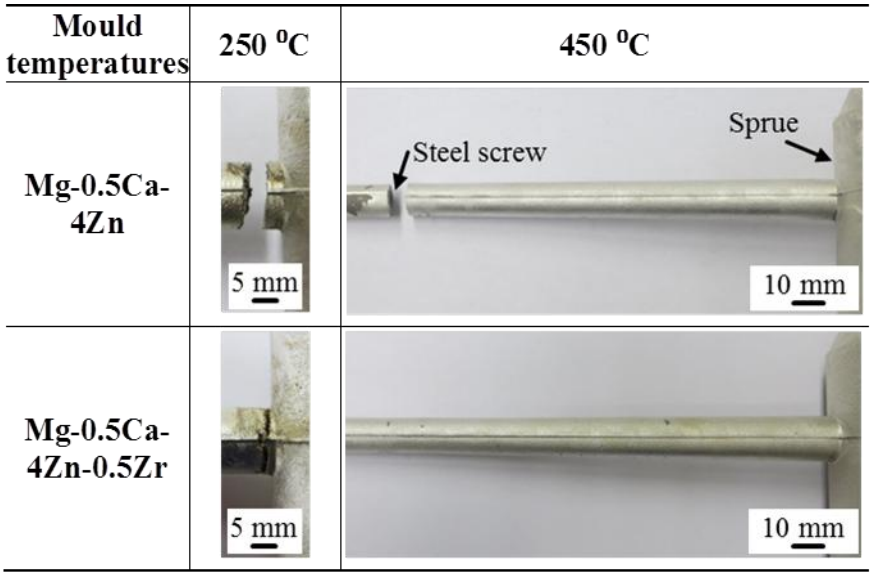

Fig. 14. Macro photographs of the hot tears for Mg-0.5Ca-4Zn and Mg-0.5Ca-4Zn-0.5Zr alloys cast at both mould temperatures.

Figure 15

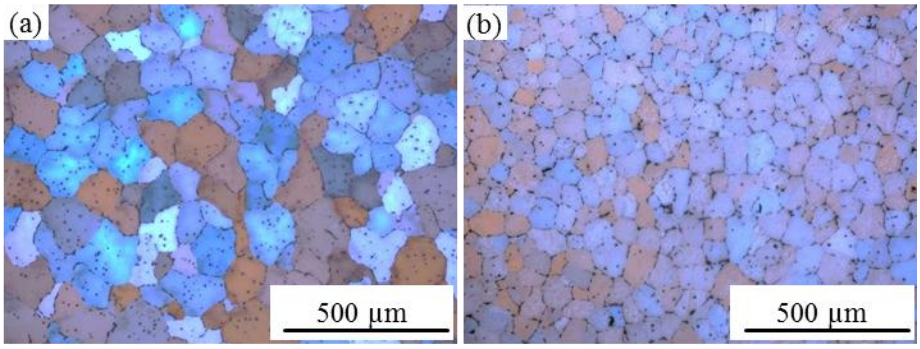

Fig. 15. Grain structures at the sprue-rod junction for alloys cast at a mould temperature of 250 ^{0}C, (a) Mg-0.5Ca-4Zn, (b) Mg-0.5Ca-4Zn-0.5Zr

Figure 16

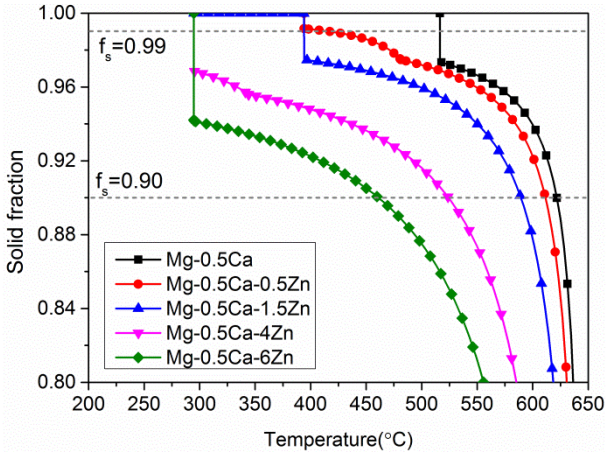

Fig. 16. Solid fraction as a function of temperature for Mg-0.5Ca-xZn alloys calculated with Pandat Software.

Figure 17

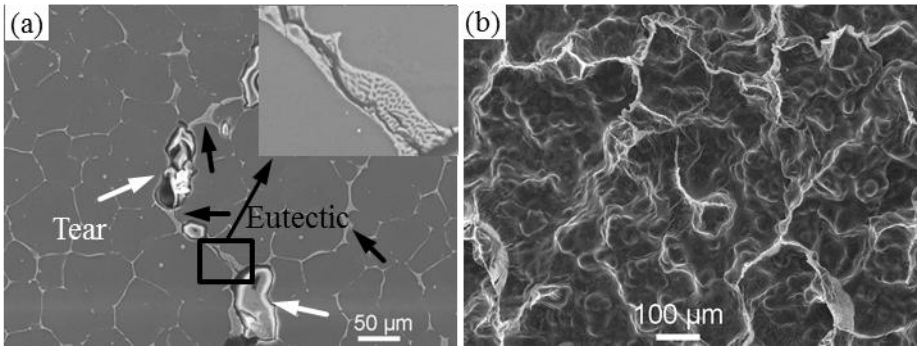

Fig. 17. (a) Microstructure of the cross sections, (b) fracture surface of hot tears for Mg-0.5Ca-4Zn-0.5Zr alloys cast at T_{mould} = 250 ^{0}C.